Available online at www.sciencedirect.com
SCIENCE DIRECT®
Journal of Organometallic Chemistry 678 (2003) 72–81
Journal of Organometallic Chemistry
www.elsevier.com/locate/jorganchem

Mixed-metal cluster chemistry. 24[1]. Isocyanide derivatives of $[MoIr_3(\mu\text{-}CO)_3(CO)_8(\eta\text{-}C_5H_5)]$ and $[Mo_2Ir_2(\mu\text{-}CO)_3(CO)_7(\eta\text{-}C_5H_5)_2]$; X-ray crystal structures of $[MoIr_3(\mu\text{-}CO)_3(CO)_7(L)(\eta\text{-}C_5H_5)]$ (L = $CNBu^t$, $CNC_6H_3Me_2$-2,6) and $[Mo_2Ir_2(\mu\text{-}CO)_2(CNBu^t)_2(CO)_6(\eta\text{-}C_5H_5)_2]$

Alistair J. Usher [a], Mark G. Humphrey [a,*], Anthony C. Willis [b]

[a] Department of Chemistry, Australian National University, Canberra, ACT 0200, Australia
[b] Research School of Chemistry, Australian National University, Canberra, ACT 0200, Australia

Received 25 March 2003; received in revised form 7 May 2003; accepted 7 May 2003

Abstract

Reactions of $MoIr_3(\mu\text{-}CO)_3(CO)_8(\eta\text{-}C_5H_5)$ (**1**) with stoichiometric amounts of isocyanides afford the ligand-substituted clusters $[MoIr_3(\mu\text{-}CO)_3(CO)_{8-n}(L)_n(\eta\text{-}C_5H_5)]$ (L = $CNBu^t$, $n = 1$ (**3**), 2 (**4**), 3 (**5**); L = $CNC_6H_3Me_2$-2,6, $n = 1$ (**6**), 2 (**7**), 3 (**8**)) in moderate to excellent yields (13–75%). Single-crystal X-ray studies of **3** and **6** reveal that the isocyanides occupy coordination sites on an apical cluster core metal atom, a first for ligand-substituted derivatives of **1**. In contrast, reaction of $Mo_2Ir_2(\mu\text{-}CO)_3(CO)_7(\eta\text{-}C_5H_5)_2$ (**2**) with one or two equivalents of $CNBu^t$ affords $Mo_2Ir_2(\mu\text{-}CO)_2(CNBu^t)_2(CO)_6(\eta\text{-}C_5H_5)_2$ (**9**) as the only major product. A single-crystal X-ray study of **9** reveals an unprecedented carbonyl configuration about the pseudotetrahedral cluster core.

Keywords: Molybdenum; Iridium; Carbonyl; Isocyanide; Cyclopentadienyl; Cluster

1. Introduction

Mixed-metal clusters are of interest for several reasons. A polar metal–metal bond can enhance co-operative effects between adjacent metal centres; these clusters can be precursors for catalytically active species with well-defined metal:metal stoichiometry, and the differing metals may provide useful labels for ligand fluxionality studies [2]. Also of interest is the possibility of metallo- and site-selectivity upon reaction with specific reagents. The phosphine and phosphite chemistry of Group 6 iridium clusters has been studied extensively [2–12], but isocyanide chemistry has been little investigated, the sole report comprising reactivity studies of the tetrahedral cluster $WIr_3(CO)_{11}(\eta\text{-}C_5H_5)$ towards Bu^tNC and $CNC_6H_3Me_2$-2,6 [13]; there are no reports thus far of the isocyanide chemistry of mixed molybdenum–iridium clusters.

$MoIr_3(\mu\text{-}CO)_3(CO)_8(\eta\text{-}C_5H_5)$ (**1**) is related to $WIr_3(CO)_{11}(\eta\text{-}C_5H_5)$ by (conceptual) Group 6 metal replacement and a rearrangement of carbonyl distribution in the crystallographically characterized form to embrace a plane of bridging carbonyls about a $MoIr_2$ face, while $Mo_2Ir_2(\mu\text{-}CO)_3(CO)_7(\eta\text{-}C_5H_5)_2$ (**2**) is conceptually related to **1** by isolobal replacement of one $Ir(CO)_3$ vertex by a $Mo(CO)_2(\eta\text{-}C_5H_5)$ unit. We report herein the results of a study into the isocyanide chemistry of **1** and **2**, and the X-ray structural characterization of three products, one of which contains a heretofore unobserved carbonyl distribution for a tetrahedral cluster.

* Corresponding author. Tel.: +61-2-6125-2927; fax: +61-2-6125-0760.
E-mail address: mark.humphrey@anu.edu.au (M.G. Humphrey).
[1] For Part 22, see [1].

0022-328X/03/$ - see front matter © 2003 Published by Elsevier B.V.
doi:10.1016/S0022-328X(03)00438-8

Table 1
Product distributions obtained from reactions of isocyanides with **1**

Ligand	Product yields (%)		
	$MoIr_3(CO)_{10}(L)(\eta\text{-}C_5H_5)$	$MoIr_3(CO)_9(L)_2(\eta\text{-}C_5H_5)$	$MoIr_3(CO)_8(L)_3(\eta\text{-}C_5H_5)$
1 equivalent of ^{t}BuNC	32	–	–
2 equivalents of ^{t}BuNC	49	23	2
3 equivalents of ^{t}BuNC	–	75	14
1 equivalent of *m*-XyNC	49	2	–
2 equivalents of *m*-XyNC	14	64	17

2. Results and discussion

2.1. Synthesis and characterization of $MoIr_3(\mu\text{-}CO)_3(CO)_{8-n}(L)_n(\eta\text{-}C_5H_5)$ ($n = 1, 2, 3$; $L = CNBu^t$, $CNC_6H_3Me_2$-2,6 (**3**–**8**))

The reactions of **1** with n equivalents of RNC ($n = 1$, 2, 3; $R = Bu^t$, $CNC_6H_3Me_2$-2,6) proceed in CH_2Cl_2 or THF at room temperature. The product distributions obtained are shown in Table 1.

Reaction with one equivalent of isocyanide produces the expected mono-substituted adduct $MoIr_3(CNR)(CO)_{10}(\eta\text{-}C_5H_5)$ for both Bu^tNC and $CNC_6H_3Me_2$-2,6 (**3** and **6**, respectively), together with a small amount of the bis-substituted adduct $MoIr_3(CNR)_2(CO)_9(\eta\text{-}C_5H_5)$ in the case of $CNC_6H_3Me_2$-2,6 (**7**). Reaction with two equivalents yields a mixture of mono-, bis- and tris-substituted adducts; this is in contrast to the heavier tungsten-containing congeners which display almost stepwise substitution reactions [13]. The highly substituted clusters $MoIr_3(CO)_8(L)_3(\eta\text{-}C_5H_5)$ ($L = Bu^tNC$ (**5**), $CNC_6H_3Me_2$-2,6 (**8**)) were found to be unstable in solution at 3 °C, with **8** decomposing much more rapidly than the sterically less encumbered Bu^tNC-containing derivative. Reaction of **1** with three equivalents (and excess) of $CNC_6H_3Me_2$-2,6 was therefore not attempted due to the observed instability of the highly substituted products.

The clusters $MoIr_3(CO)_{11-n}(L)_n(\eta\text{-}C_5H_5)$ ($n = 1$, 2; $L = Bu^tNC$, $CNC_6H_3Me_2$-2,6) were characterized by IR, ^{1}H-NMR spectroscopy, MS and satisfactory microanalysis. Due to the aforementioned instability, the tris-substituted cluster **5** was characterized by IR, ^{1}H-NMR spectroscopy and MS, while **8** decomposed rapidly and was tentatively identified by solution IR. All compounds display bands corresponding to edge bridging carbonyl ligands in their solution IR spectra, the number of bands in the ν(CO) region being consistent with the presence of isomers. The identity of one isomer of each of **3** and **6** was confirmed by X-ray structural studies. The ^{1}H-NMR spectra contain resonances in the cyclopentadienyl and methyl regions in the predicted ratios, and a phenyl multiplet in the case of the $CNC_6H_3Me_2$-2,6-containing derivatives. The mass spectra contain molecular ions at the expected m/z values and fragmentation by loss of carbonyl ligands, the latter becoming competitive with loss of methyl groups from both $CNC_6H_3Me_2$-2,6 and Bu^tNC ligands in some cases.

2.2. X-ray structural studies of $MoIr_3(\mu\text{-}CO)_3(CO)_7(L)(\eta\text{-}C_5H_5)$ ($L = Bu^tNC$ (**3**), $CNC_6H_3Me_2$-2,6 (**6**))

One isomer of each of **3** and **6** was subjected to X-ray diffraction analysis; the solid-state molecular structures and atomic labelling schemes are shown in Figs. 1 and 2, respectively [14]. Relevant crystal data and structure refinement details for the structural studies are collected

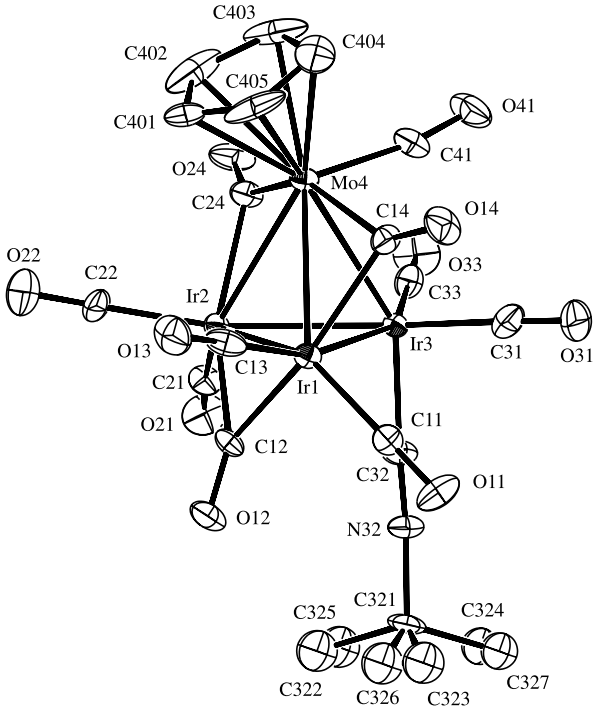

Fig. 1. ORTEP [14] plot and atomic numbering scheme for $MoIr_3(\mu\text{-}CO)_3(CNBu^t)(CO)_7(\eta\text{-}C_5H_5)$ (**3**). Each methyl group of the Bu^tNC ligand is disordered over two sites. Displacement ellipsoids are at the 30% probability level. Hydrogen atoms have been omitted for clarity.

in Table 2, while selected bond lengths and angles for each structure are listed in Tables 3 and 4, respectively.

Both complexes share the $MoIr_3$ pseudotetrahedral framework of the parent cluster **1** and possess three bridging carbonyls arranged about a $MoIr_2$ plane, a molybdenum-bound η^5-cyclopentadienyl group inclined towards the plane of bridging carbonyls and *trans* to the longest Mo–Ir bond, seven terminal carbonyl ligands and a terminal isocyanide ligand attached to the apical iridium atom. In both cases, the $MoIr_3$ core distances (Ir–Ir_{ave} 2.69 Å; Mo–Ir_{ave} 2.87 Å for **3** and Ir–Ir_{ave} 2.70 Å; Mo–Ir_{ave} 2.87 Å for **6**) are very similar to those of the parent cluster **2** (Ir–Ir_{ave} 2.70 Å; Mo–Ir_{ave} 2.86 Å), with the carbonyl bridged M–M vectors shorter than the non-bridged cluster core bonds.

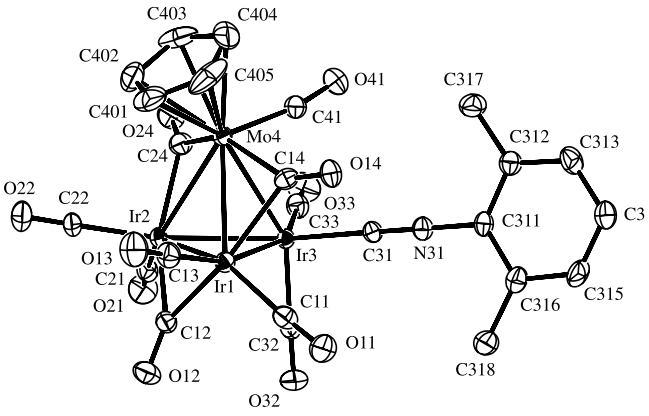

Fig. 2. ORTEP [14] plot and atomic numbering scheme for $MoIr_3(\mu\text{-}CO)_3(CNC_6H_3Me_2\text{-}2,6)(CO)_7(\eta\text{-}C_5H_5)$ (**6**). Displacement ellipsoids are at the 30% probability level. Hydrogen atoms have been omitted for clarity.

2.3. Synthesis and characterization of $Mo_2Ir_2(\mu\text{-}CO)_2(CNBu^t)_2(CO)_6(\eta\text{-}C_5H_5)_2$ (**9**)

The reactions of **2** with *n* equivalents of Bu^tNC ($n = 1$ or 2) proceed in CH_2Cl_2 at room temperature. Reaction with one equivalent affords only one major band during chromatographic work up, identified as the unexpected bis-substituted cluster adduct $Mo_2Ir_2(\mu\text{-}CO)_2(CNBu^t)_2(CO)_6(\eta\text{-}C_5H_5)_2$ (**9**) in good yield. Similarly, reaction with two equivalents affords the same major product and small amounts of other unstable, uncharacterizable material.

Table 2
Crystal data and structure refinement details for **3**, **6** and **9**

	3	**6**	**9**
Empirical formula	$C_{20}H_{14}Ir_3MoNO_{10}$	$C_{24}H_{14}Ir_3MoNO_{10}$	$C_{28}H_{28}Ir_2Mo_2N_2O_8$
Formula weight	1100.93	1148.98	1096.86
Crystal size (mm^3)	$0.45 \times 0.18 \times 0.10$	$0.22 \times 0.20 \times 0.16$	$0.22 \times 0.18 \times 0.13$
Colour, habit	orange, plate	orange, block	black, plate
Crystal system	monoclinic	monoclinic	monoclinic
Space group	$P2_1/n$	$P2_1/n$	$C2/c$
Unit cell dimensions			
a (Å)	8.8024(1)	12.8280(1)	22.2568(4)
b (Å)	18.2985(3)	11.5305(1)	9.5332(2)
c (Å)	15.5277(3)	18.8762(2)	16.5962(3)
α (°)	90	90	90
β (°)	90.1576(8)	105.0161(7)	117.1281(9)
γ (°)	90	90	90
V ($Å^3$)	2501.05(7)	2696.70(4)	3133.97(11)
Z	4	4	4
D_{calc} ($g\,cm^{-3}$)	2.924	2.830	2.325
μ (mm^{-1})	16.45	15.27	9.30
θ_{max} (°)	30	30	27.5
Temperature (K)	200	200	293
N_{cell}	73 359	60 634	24 526
$N_{collected}$	56 034	71 123	32 659
N_{unique}	7305	7882	3601
N_{obs}	2929 ($I > 3.00\sigma(I)$)	4077 ($I > 3.00\sigma(I)$)	2190 ($I > 2.00\sigma(I)$)
Absorption correction	integration	integration	integration
T_{min}, T_{max}	0.056, 0.408	0.063, 0.176	0.206, 0.373
No. of parameters	311	353	191
R [a]	0.0314	0.0201	0.0216
R_w [b]	0.0344	0.023	0.0215
S	1.07	1.07	1.08
$(\Delta/\rho)_{min}$ ($e\,Å^{-3}$)	−1.52	−0.81	−0.6
$(\Delta/\rho)_{max}$ ($e\,Å^{-3}$)	2.49	0.86	0.81

[a] $R = \Sigma||F_0| - |F_c||/\Sigma|F_0|$.
[b] $R_w = [(\Sigma w(|F_0| - |F_c|)^2/\Sigma wF_0^2)]^{1/2}$.

Table 3
Selected bond lengths (Å) and angles (°) for $MoIr_3(\mu\text{-}CO)_3(CNBu^t)(CO)_7(\eta\text{-}C_5H_5)$

Bond length			
Ir1–Ir2	2.6953(6)	Mo4–C24	2.163(12)
Ir1–Ir3	2.6917(6)	Mo4–C41	1.955(14)
Ir1–Mo4	2.845(1)	Mo4–C401	2.33(2)
Ir1–C11	1.885(12)	Mo4–C402	2.326(18)
Ir1–C12	2.090(11)	Mo4–C403	2.261(15)
Ir1–C13	1.882(14)	Mo4–C404	2.235(15)
Ir1–C14	2.158(13)	Mo4–C405	2.281(15)
Ir2–Ir3	2.6920(6)	O11–C11	1.146(15)
Ir2–Mo4	2.864(1)	O12–C12	1.148(14)
Ir2–C12	2.104(11)	O13–C13	1.145(16)
Ir2–C21	1.905(11)	O14–C14	1.174(14)
Ir2–C22	1.895(14)	O21–C21	1.123(15)
Ir2–C24	2.157(12)	O22–C22	1.166(17)
Ir3–Mo4	2.8909(11)	O24–C24	1.156(15)
Ir3–C31	1.893(15)	O31–C31	1.141(17)
Ir3–C32	1.959(12)	O33–C33	1.122(16)
Ir3–C33	1.918(14)	O41–C41	1.137(17)
Mo4–C14	2.136(12)	N32–C32	1.146(16)
Bond angle			
Ir2–Ir1–Ir3	59.964(16)	Ir1–Mo4–C24	103.7(3)
Ir2–Ir1–Mo4	62.19(2)	Mo4–Ir1–C14	48.2(3)
Ir3–Ir1–Mo4	62.87(2)	Ir1–C11–O11	173.9(12)
Ir1–Ir2–Ir3	59.952(16)	Ir1–C12–O12	140.9(10)
Ir1–Ir2–Mo4	61.48(2)	Ir2–C12–O12	139.0(10)
Ir3–Ir2–Mo4	62.61(2)	Ir1–C13–O13	176.6(12)
Ir1–Ir3–Ir2	60.084(16)	Ir1–C14–O14	133.3(10)
Ir1–Ir3–Mo4	61.16(2)	Ir2–C21–O21	175.1(13)
Ir2–Ir3–Mo4	61.61(2)	Ir2–C22–O22	178.2(13)
Ir1–Mo4–Ir2	56.34(2)	Ir2–C24–O24	133.4(10)
Ir1–Mo4–Ir3	55.96(2)	Ir3–C31–O31	178.6(14)
Ir2–Mo4–Ir3	55.78(2)	Ir3–C33–O33	178.6(13)
Ir1–Ir2–C12	49.8(3)	Ir3–C32–N32	177.0(12)
Ir2–Ir1–C12	50.2(3)	Mo4–C14–O14	143.7(11)
Mo4–Ir2–C24	48.6(3)	Mo4–C24–O24	143.5(10)
Ir2–Mo4–C24	48.4(3)		

Table 4
Selected bond lengths (Å) and angles (°) for $MoIr_3(\mu\text{-}CO)_3(CNC_6H_3Me_2\text{-}2,6)(CO)_7(\eta\text{-}C_5H_5)$

Bond length			
Ir1–Ir2	2.7037(3)	Mo4–C24	2.152(7)
Ir1–Ir3	2.6980(3)	Mo4–C41	1.959(7)
Ir1–Mo4	2.8367(6)	Mo4–C401	2.344(9)
Ir1–C11	1.898(7)	Mo4–C402	2.313(8)
Ir1–C12	2.099(6)	Mo4–C403	2.285(8)
Ir1–C13	1.888(7)	Mo4–C404	2.287(8)
Ir1–C14	2.220(6)	Mo4–C405	2.319(8)
Ir2–Ir3	2.6920(3)	O11–C11	1.127(8)
Ir2–Mo4	2.8568(5)	O12–C12	1.155(8)
Ir2–C12	2.117(6)	O13–C13	1.135(8)
Ir2–C21	1.894(7)	O14–C14	1.170(7)
Ir2–C22	1.897(6)	O21–C21	1.128(8)
Ir2–C24	2.145(7)	O22–C22	1.128(8)
Ir3–Mo4	2.9031(6)	O24–C24	1.167(8)
Ir3–C31	1.986(5)	O32–C32	1.116(8)
Ir3–C32	1.911(6)	O33–C33	1.125(8)
Ir3–C33	1.930(7)	O41–C41	1.152(8)
Mo4–C14	2.107(6)	N31–C31	1.150(7)
Bond angle			
Ir2–Ir1–Ir3	59.785(8)	Ir1–Mo4–C24	103.82(18)
Ir2–Ir1–Mo4	62.023(12)	Mo4–Ir1–C14	47.33(16)
Ir3–Ir1–Mo4	63.216(13)	Ir1–C11–O11	177.1(6)
Ir1–Ir2–Ir3	60.001(8)	Ir1–C12–O12	141.6(5)
Ir1–Ir2–Mo4	61.275(13)	Ir2–C12–O12	138.7(5)
Ir3–Ir2–Mo4	63.012(12)	Ir1–C13–O13	178.2(7)
Ir1–Ir3–Ir2	60.214(9)	Ir1–C14–O14	130.4(5)
Ir1–Ir3–Mo4	60.725(13)	Ir2–C21–O21	177.4(6)
Ir2–Ir3–Mo4	61.267(12)	Ir2–C22–O22	179.0(6)
Ir1–Mo4–Ir2	56.701(12)	Ir2–C24–O24	133.1(5)
Ir1–Mo4–Ir3	56.059(12)	Ir3–C31–N31	179.1(6)
Ir2–Mo4–Ir3	55.721(11)	Ir3–C32–O32	178.4(6)
Ir1–Ir2–C12	49.83(17)	Ir3–C33–O33	179.1(6)
Ir2–Ir1–C12	50.42(17)	Mo4–C14–O14	147.7(5)
Mo4–Ir2–C24	48.44(17)	Mo4–C24–O24	143.5(5)
Ir2–Mo4–C24	48.23(18)		

The cluster product **9** was characterized by a combination of IR, ^{1}H-NMR spectroscopy, FABMS and satisfactory microanalysis. The solution IR spectrum of the complex contains one major ν(NC) band accompanied by minor shoulders and ν(CO) bands spread throughout the terminal and bridging carbonyl regions. The number of ν(CO) and ν(NC) bands in the spectrum is indicative of the presence of isomers in solution. The ^{1}H-NMR spectrum contains resonances in the *tert*-butyl and cyclopentadienyl regions in the expected ratios. The mass spectrum contains a molecular ion at the expected m/z value and fragment ions corresponding to the sequential loss of all carbonyl ligands. Competitive fragmentation by loss of pairs of methyl groups is also observed but is not distinguishable from loss of carbonyl ligands due to the wide isotope pattern of the Mo_2Ir_2 core. Cluster **9** was subjected to a single-crystal X-ray diffraction study.

2.4. X-ray structural study of $Mo_2Ir_2(\mu\text{-}CO)_2(CNBu^t)_2(CO)_6(\eta\text{-}C_5H_5)_2$ (9)

The X-ray crystal structure and atomic numbering scheme of $[MoIr(\mu\text{-}CO)(CNBu^t)(CO)_3(\eta\text{-}C_5H_5)]_2$ (**9**) with imposed C_{2v} symmetry is shown in Fig. 3. Relevant crystal data and structure refinement details for the structural studies are collected in Table 2, while selected interatomic bond lengths and angles are listed in Table 5.

The cluster possesses an unusual carbonyl disposition but the core itself shares a number of structural similarities with the parent cluster **2**. The cluster retains the pseudotetrahedral core geometry with each molybdenum atom bearing one η^5-cyclopentadienyl group. All intra-core bond angles are close to 60°, as expected, with those centred on an iridium atom slightly larger than those centred on a molybdenum atom, a similar trend being observed in the unsubstituted parent cluster core.

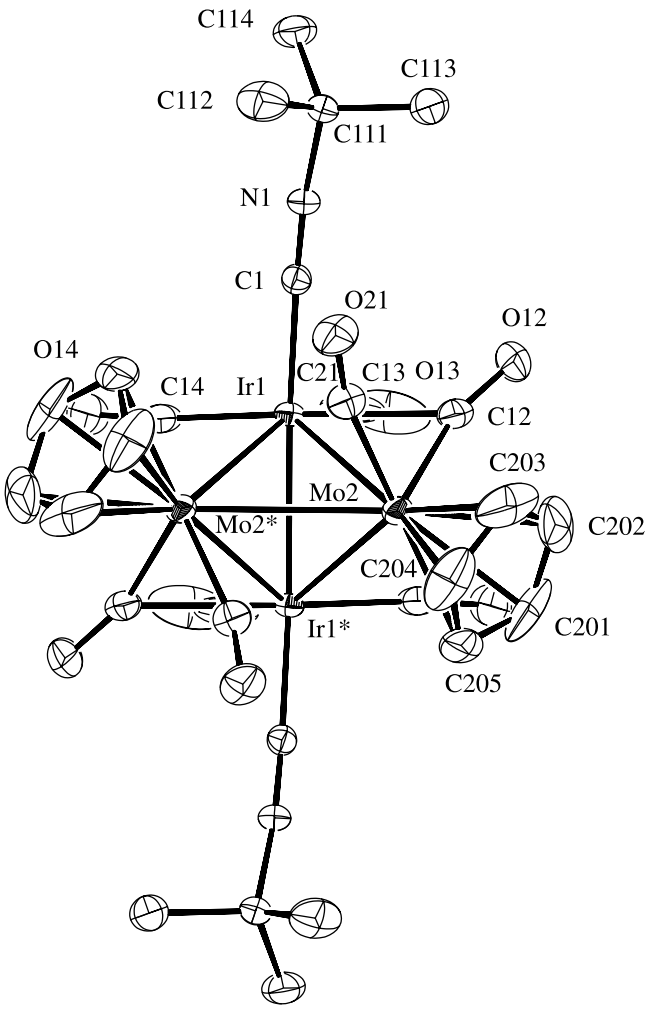

Fig. 3. ORTEP [14] plot and atomic numbering scheme for [MoIr(μ-CO)(CNBu^t)(CO)$_3$(η-C$_5$H$_5$)]$_2$ (**9**). Displacement ellipsoids are at the 20% probability level. Hydrogen atoms have been omitted for clarity.

Table 5
Selected bond lengths (Å) and angles (°) for [MoIr(μ-CO)(CNBu^t)(CO)$_3$(η-C$_5$H$_5$)]$_2$

Bond length		Bond angle	
Ir1–Ir1^a	2.6761(4)	Ir1^a–Ir1–Mo2	62.112(12)
Ir1–Mo2	2.8726(6)	Ir1^a–Ir1–Mo2^a	62.309(11)
Ir1–Mo2^a	2.8674(6)	Mo2–Ir1–Mo2^a	63.78(2)
Mo2–Mo2^a	3.032(1)	Ir1–Mo2–Ir1^a	55.579(12)
Ir1–C1	1.979(6)	Ir1–Mo2–Mo2^a	58.027(13)
N1–C1	1.153(7)	Ir1^a–Mo2–Mo2^a	58.194(14)
Ir1–C12	2.477(7)	Ir1–C1–N1	177.3(5)
Ir1–C13	1.847(9)	Ir1–C12–O12	121.9(6)
Ir1–C14	1.865(8)	Ir1–C13–O13	174.0(8)
Mo2–C12	1.962(7)	Ir1–C14–O14	166.1(9)
Mo2–C21	1.969(7)	Mo2–C12–O12	158.2(7)
		Mo2–C21–O21	166.1(6)

[a] Atom generated by the symmetry operation $(1-x, y, 3/2-z)$.

The Ir–Ir and Ir–Mo bond distances are within the range observed in both the Mo$_2$Ir$_2$(μ-CO)$_3$(CO)$_7$(η-C$_5$H$_5$)$_2$ (**2**) and MoIr$_3$(μ-CO)$_3$(CO)$_8$(η-C$_5$H$_5$) (**1**) clusters, but the Mo–Mo bond distance (3.032(1) Å) is shorter than in **2** (3.112(1) Å) and more consistent with the expected atomic radius for molybdenum of 1.50 Å [15].

To the best of our knowledge, the carbonyl distribution about the core is unprecedented for a tetrahedral mixed-metal cluster. The plane of bridging carbonyls present in the parent cluster is absent in **9** and descriptions of ligand substitution sites used to date cannot be applied [4]. No carbonyl ligands are formally fully bridging as defined by the Curtis asymmetry factor [16,17], yet most have a significant semi-bridging character with $0.26 < \alpha < 0.71$ and only two are co-ordinated in a fully terminal manner, one to each iridium atom. This widens the range of available coordination sites from the three relatively rigid radial, axial and apical sites of the parent cluster and allows projection of the cyclopentadienyl groups as far as possible from one another. This disposition eases steric crowding around the Mo–Mo bond, resulting in a shorter bond length than that in the parent cluster.

2.5. Synthesis and characterization of Mo$_2$Ir$_2$(CNC$_6$H$_3$Me$_2$-2,6)$_n$(CO)$_{10-n}$(η-C$_5$H$_5$)$_2$ ($n = 1$ (**10**), 2 (**11**))

The reaction of **2** with two equivalents of CNC$_6$H$_3$Me$_2$-2,6 also proceeds in CH$_2$Cl$_2$ at room temperature but does not proceed in an analogous manner to the reaction with Bu^{t}NC. A product distribution of Mo$_2$Ir$_2$(CNC$_6$H$_3$Me$_2$-2,6)$_n$(CO)$_{10-n}$(η-C$_5$H$_5$)$_2$ ($n = 0$, 1, 2) was obtained, in contrast to the single major Bu^{t}NC-containing product.

Mo$_2$Ir$_2$(CNC$_6$H$_3$Me$_2$-2,6)(CO)$_9$(η-C$_5$H$_5$)$_2$ (**10**) was characterized by a combination of solution IR, ^{1}H-NMR spectroscopy, FABMS and satisfactory microanalysis. The IR spectrum contains a single band in the ν(NC) region and a large number of ν(CO) bands in the terminal and bridging carbonyl regions. The number of bands in the ν(CO) region is indicative of the presence of isomers in solution. The ^{1}H-NMR spectrum contains resonances in the methyl, phenyl and cyclopentadienyl regions in the expected ratios and the mass spectrum contains a molecular ion at the expected m/z value and fragment ions corresponding to the loss of all carbonyls becoming competitive with loss of methyl groups from $[M-8CO]^+$.

The cluster Mo$_2$Ir$_2$(CNC$_6$H$_3$Me$_2$-2,6)$_2$(CO)$_8$(η-C$_5$H$_5$)$_2$ (**11**) did not behave analogously to its Bu^{t}NC analogue and was found to decompose rapidly in solution, yielding **10** and an uncharacterizable brown

residue. The cluster was tentatively identified by solution IR but could not be separated from the decomposition products.

2.6. Discussion

The results of the studies described above can be contrasted with those in our earlier report dealing with tungsten — tri-iridium cluster — isocyanide chemistry [13]. Reactions at the tungsten-containing cluster proceed in a stepwise fashion, whereas the more reactive molybdenum-containing congener reacts to afford a range of products with varying levels of ligand substitution centred on the stoichiometric product for *m*-xylylisocyanide and a lower level of substitution for *tert*-butylisocyanide. In our tungsten-containing cluster study, we reported the structural characterization of $WIr_3(CNC_6H_3Me_2\text{-}2,6)_2(CO)_9(\eta\text{-}C_5H_5)$, with an all-terminal carbonyl geometry and both isocyanides coordinated at the same iridium atom, *trans* to Ir–Ir bonds. This study has afforded the first structurally characterized mono-isocyanide products from the Group 6 iridium system, the product clusters containing a $MoIr_2$ plane of bridging carbonyls and the isocyanide ligated in a terminal manner at the apical iridium atom; whereas the *m*-xylylisocyanide ligand is found *trans* to an Ir–Ir bond, the *tert*-butylisocyanide is ligated *trans* to the Mo–Ir linkage. Although no report of the reactivity of $W_2Ir_2(CO)_{10}(\eta\text{-}C_5H_5)_2$ towards isocyanides is extant, phosphine substitution studies have been reported in both the ditungsten–diiridium [9,11] and the dimolybdenum–diiridium [6] systems. The *m*-xylylisocyanide chemistry in the present report is entirely analogous, affording a stable mono-substituted product and an unstable/significantly less stable di-substituted product. In contrast, *tert*-butylisocyanide reacts with $Mo_2Ir_2(CO)_{10}(\eta\text{-}C_5H_5)_2$ in an unprecedented manner to afford a bis-substituted cluster product only, which is stable, and which possesses a previously unknown carbonyl ligand distribution for these clusters.

3. Experimental

Reactions were performed under an atmosphere of dry dinitrogen (available in-house from liquid nitrogen boiloff) using standard Schlenk techniques [18]. Most cluster complexes proved to be indefinitely stable in air as solids and for at least short periods of time in solution, and thus no precautions were taken to exclude air in their manipulation. All reaction solvents used were analytical reagent (AR) grade. The reaction solvents were dried and distilled under dry nitrogen using standard methods: CH_2Cl_2 over CaH_2; THF over sodium benzophenone ketyl. Petroleum refers to a petroleum fraction of boiling range 60–80 °C. Cyclopentadiene was cracked from dicyclopentadiene dimer (Aldrich) immediately prior to use. The isocyanides Bu^tNC and $CNC_6H_3Me_2$-2,6 (Aldrich) were used as received. Literature procedures (or minor modifications thereof) were used to synthesize **1** and **2** [19].

Cluster products were purified by thin-layer chromatography (TLC) on 20 cm × 20 cm glass plates coated with Merck GF_{254} silica gel (0.5 mm). Analytical TLC, used for monitoring the extent of reaction, was carried out on aluminium sheets coated with 0.25 mm silica gel.

Infrared spectra were recorded on a Perkin–Elmer System 2000 FT-IR with CaF_2 solution cells; spectral frequencies are recorded in cm^{-1}. All analytical spectra were recorded as solutions in cyclohexane or CH_2Cl_2 (AR grade). ^1H spectra were recorded in $CDCl_3$ or acetone-d_6 (Cambridge Isotope Laboratories) using a Varian Gemini-300 spectrometer (at 300 MHz) and are referenced to residual non-deuterated solvent peaks: $CHCl_3$ at 7.24 ppm and acetone at 2.04 ppm. Secondary ion mass spectra (SIMS) and fast atom bombardment mass spectra (FABMS) were recorded using a VG ZAB 2SEQ instrument (30 kV Cs^+ ions, current 1 mA, accelerating potential 8 kV, 3-nitrobenzyl alcohol matrix) at the Research School of Chemistry, Australian National University, or the Department of Chemistry, University of Western Australia. All MS were calculated with *m*/*z* based on ^{96}Mo and ^{192}Ir assignments, and are reported in the form: *m*/*z* (assignment, relative intensity). Elemental microanalyses were carried out by the Microanalysis Service Unit in the Research School of Chemistry, Australian National University.

3.1. Reaction of $MoIr_3(CO)_{11}(\eta\text{-}C_5H_5)$ with one equivalent of Bu^tNC

Bu^tNC (4 μl, 0.04 mmol) was added to an orange solution of **1** (38.0 mg, 0.036 mmol) in CH_2Cl_2 (20 ml) and stirred at rt for 16 h. The resulting orange solution was reduced to dryness in vacuo, the residue redissolved in a minimum of CH_2Cl_2 (ca. 1 ml) and applied to preparative TLC plates. Elution with CH_2Cl_2–petroleum (1/2) gave two bands. The contents of the first band ($R_f = 0.68$) were identified as unreacted **1** (26.1 mg, 0.025 mmol, 65%) by solution IR. The contents of the second band ($R_f = 0.54$) were crystallized from CH_2Cl_2–MeOH to afford orange crystals identified as $MoIr_3(\mu\text{-}CO)_3(CNBu^t)(CO)_7(\eta\text{-}C_5H_5)$ (**3**) (13.3 mg, 0.012 mmol, 32%). A crystal grown by this method was selected for a single-crystal X-ray structural study. IR ($c\text{-}C_6H_{12}$): ν(NC) 2184m, ν(CO) 2089w, 2063vs, 2048m, 2036vs, 2033vs, 2019w, 2008vs, 1994vs, 1984w, 1907sh, 1884m, 1840w, 1798m, 1777m, 1767s cm^{-1}. ^1H-NMR (acetone-d_6): δ 5.32 (s, 5H, C_5H_5), 1.51 (s, 9H, Bu^tNC) ppm. MS (SI): 1101 ($[M]^+$, 23), 1073 ($[M-CO]^+$, 8), 1045 ($[M-2CO]^+$, 44), 1017 ($[M-3CO]^+$, 100), 989 ($[M-4CO]^+$, 29), 961 ($[M-5CO]^+$, 20), 933 ($[M-6CO]^+$, 16), 905

([M−7CO]$^+$, 13), 877 ([M−8CO]$^+$, 5), 849 ([M−9CO]$^+$, 2). Anal. Found: C, 21.83; H, 1.08; N, 1.41. $C_{20}H_{14}Ir_3MoNO_{10}$ Calc: C, 21.82; H, 1.28; N, 1.27%.

3.2. Reaction of $MoIr_3(CO)_{11}(\eta\text{-}C_5H_5)$ with two equivalents of Bu^tNC

Following the procedure of Section 3.1, Bu^tNC (4 μl, 0.04 mmol) and $MoIr_3(CO)_{11}(\eta\text{-}C_5H_5)$ (19.0 mg, 0.018 mmol) in CH_2Cl_2 (20 ml) afforded a mixture which was applied to preparative TLC plates after 16 h reaction. Elution with CH_2Cl_2–petroleum (1/2) gave three bands. The contents of the first band ($R_f = 0.48$) were identified as **3** (9.8 mg, 0.0089 mmol, 49%) by solution IR. The contents of the second band ($R_f = 0.32$) were crystallized from $CHCl_3$–MeOH to afford a yellow polycrystalline material identified as $MoIr_3(CNBu^t)_2(CO)_9(\eta\text{-}C_5H_5)$ (**4**) (4.8 mg, 0.0041 mmol, 23%). IR (c-C_6H_{12}): ν(NC) 2181m, 2154m, ν(CO) 2069w, 2049s, 2025vs, 2007vs, 1998s, 1988vs, 1978m, 1881m, 1853m, 1840m, 1801m, 1793m, 1769s cm^{-1}. ^{1}H-NMR (acetone-d_6): δ 5.13 (s, 5H, C_5H_5), 1.48 (s, 18H, Bu^tNC) ppm. MS (FAB): 1156 ([M]$^+$, 16), 1128 ([M−CO]$^+$, 5), 1100 ([M−2CO]$^+$, 36), 1072 ([M−3CO]$^+$, 100), 1044 ([M−4CO]$^+$, 34), 1016 ([M−5CO]$^+$, 22), 988 ([M−6CO]$^+$, 19), 960 ([M−7CO]$^+$, 9). MS (SI): 1156 ([M]$^+$, 28), 1128 ([M−CO]$^+$, 11), 1100 ([M−2CO]$^+$, 41), 1072 ([M−3CO]$^+$, 100), 1044 ([M−4CO]$^+$, 38), 1016 ([M−5CO]$^+$, 36), 988 ([M−6CO]$^+$, 12). Anal. Found: C, 24.35; H, 1.97; N, 2.28. $C_{24}H_{23}Ir_3MoN_2O_9$ Calc: C, 24.94; H, 2.01; N, 2.42%. The contents of the third band ($R_f = 0.18$) were purified by vapour diffusion of ether into a CH_2Cl_2 solution to afford a yellow powder identified as $MoIr_3(CNBu^t)_3(CO)_8(\eta\text{-}C_5H_5)$ (**5**) (0.5 mg, 0.0004 mmol, 2%). IR (CH_2Cl_2): ν(NC) 2182m, 2158s, ν(CO) 2023s, 1984vs, 1853w, 1815m, 1770sh, 1748s cm^{-1}. ^{1}H-NMR (acetone-d_6): δ 4.96 (s, 5H, C_5H_5), 1.46 (s, 27H, Bu^tNC) ppm. MS (SI): 1211 ([M]$^+$, 17), 1183 ([M−CO]$^+$, 1), 1155 ([M−2CO]$^+$, 22), 1127 ([M−3CO]$^+$, 100), 1099 ([M−4CO]$^+$, 37), 1071 ([M−5CO]$^+$, 18), 1043 ([M−6CO]$^+$, 6), 1015 ([M−7CO]$^+$, 12), 987 ([M−8CO]$^+$, 6). Microanalyses could not be obtained due to sample decomposition over days.

3.3. Reaction of $MoIr_3(CO)_{11}(\eta\text{-}C_5H_5)$ with three equivalents of Bu^tNC

Following the procedure of Section 3.1, Bu^tNC (8 μl, 0.07 mmol) and **1** (26.1 mg, 0.023 mmol) in CH_2Cl_2 (20 ml) afforded a mixture which was applied to preparative TLC plates after 16 h reaction. Elution with CH_2Cl_2–petroleum (1/2) gave two bands. The contents of the first and major band ($R_f = 0.38$) were identified as **4** (9.8 mg, 0.019 mmol, 75%) by solution IR. The contents of the second band ($R_f = 0.18$) were identified as **5** (4.2 mg, 0.0037 mmol, 14%) by solution IR.

3.4. Reaction of $MoIr_3(CO)_{11}(\eta\text{-}C_5H_5)$ with excess Bu^tNC

Following the procedure of Section 3.1, Bu^tNC (21 μl, 0.18 mmol) and **1** (30.0 mg, 0.029 mmol) in CH_2Cl_2 (20 ml) afforded a mixture which was applied to preparative TLC plates after 16 h reaction. Elution with CH_2Cl_2–petroleum (1/2) gave two bands. The contents of the first and major band ($R_f = 0.39$) were identified as **4** (17.5 mg, 0.015 mmol, 52%) by solution IR. The contents of the second band ($R_f = 0.18$) were identified as **5** (13.8 mg, 0.017 mmol, 40%) by solution IR.

3.5. Reaction of $MoIr_3(CO)_{11}(\eta\text{-}C_5H_5)$ with one equivalent of $CNC_6H_3Me_2$-2,6

Following the procedure of Section 3.1, $CNC_6H_3Me_2$-2,6 (2.5 mg, 0.018 mmol) and **1** (20.0 mg, 0.019 mmol) in CH_2Cl_2 (20 ml) afforded a mixture which was applied to preparative TLC plates after 16 h reaction. Elution with CH_2Cl_2–petroleum (3/2) gave three bands. The contents of the first band ($R_f = 0.91$) were identified as unreacted **1** (7.8 mg, 0.0074 mmol, 39%) by solution IR. The contents of the second band ($R_f = 0.83$) were crystallized from CH_2Cl_2–ethanol to afford orange crystals identified as $MoIr_3(\mu\text{-}CO)_3(CNC_6H_3Me_2\text{-}2,6)(CO)_7(\eta\text{-}C_5H_5)$ (**6**) (10.7 mg, 0.0093 mmol, 49%). A crystal grown by this method was selected for a single-crystal X-ray structural study. IR (c-C_6H_{12}): ν(NC) 2158m, ν(CO) 2075w, 2068s, 2043vs, 2039vs, 2028m, 2014s, 2003s, 1992w, 1987w, 1901w, 1864m, 1854vw, 1811w, 1785m cm^{-1}. ^{1}H-NMR (acetone-d_6): δ 7.26 (m, 3H, C_6H_3), 5.38 (s, 5H, C_5H_5), 2.40 (s, 6H, C_6Me_2) ppm. MS (FAB): 1149 ([M]$^+$, 43), 1121 ([M−CO]$^+$, 10), 1093 ([M−2CO]$^+$, 42), 1065 ([M−3CO]$^+$, 100), 1037 ([M−4CO]$^+$, 24), 1009 ([M−5CO]$^+$, 19), 981 ([M−6CO]$^+$, 25), 953 ([M−7CO]$^+$, 23), 925 ([M−8CO]$^+$, 17). Anal. Found: C, 25.02; H, 1.14; N, 1.30. $C_{24}H_{14}Ir_3MoNO_{10}$ Calc: C, 25.09; H, 1.23; N, 1.22%. The contents of the third band ($R_f = 0.78$) were crystallized from CH_2Cl_2–ethanol to afford a red amorphous solid identified as $MoIr_3(CNC_6H_3Me_2\text{-}2,6)_2(CO)_9(\eta\text{-}C_5H_5)$ (**7**) (0.5 mg, 0.0004 mmol, 2%) by solution IR.

3.6. Reaction of $MoIr_3(CO)_{11}(\eta\text{-}C_5H_5)$ with two equivalents of $CNC_6H_3Me_2$-2,6

Following the procedure of Section 3.1, $CNC_6H_3Me_2$-2,6 (5.1 mg, 0.038 mmol) and **1** (20.1 mg, 0.019 mmol) in CH_2Cl_2 (20 ml) afforded a mixture which was applied to preparative TLC plates after 16 h reaction. Elution with CH_2Cl_2–petroleum (3/2) gave four bands. The contents of the first band ($R_f = 0.86$) were identified as **6** (3.2 mg,

0.0028 mmol, 14%) by solution IR. The contents of the second band ($R_f = 0.81$) were identified as **7** (15.5 mg, 0.013 mmol, 64%). IR (c-C_6H_{12}): ν(NC) 2156m, 2125m, ν(CO) 2025s, 2042w, 2029vs, 2010m, 2002m, 1992m, 1983w, 1887w, 1853w, 1803w, 1775s cm^{-1}. ^{1}H-NMR (acetone-d_6): δ 7.22 (m, 6H, C_6H_3), 5.24 (s, 5H, C_5H_5), 2.37 (s, 12H, C_6Me_2) ppm. MS (FAB): 1252 ($[M]^+$, 14), 1224 ($[M-CO]^+$, 4), 1196 ($[M-2CO]^+$, 18), 1168 ($[M-3CO]^+$, 100), 1140 ($[M-4CO]^+$, 21), 1112 ($[M-5CO]^+$, 27), 1084 ($[M-6CO]^+$, 37), 1056 ($[M-7CO]^+$, 28), 1028 ($[M-8CO]^+$, 30). Anal. Found: C, 31.13; H, 1.95; N, 2.54. $C_{32}H_{23}Ir_3MoN_2O_9$ Calc: C, 30.70; H, 1.85; N, 2.24%. The contents of the third band ($R_f = 0.70$) were precipitated by vapour diffusion of ether into a CH_2Cl_2 solution to afford a light orange powder tentatively identified as $MoIr_3(CNC_6H_3Me_2\text{-}2,6)_3(CO)_8(\eta\text{-}C_5H_5)$ (**8**) (4.5 mg, 0.0031 mmol, 17%) which decomposed to an uncharacterizable brown residue over hours. IR (c-C_6H_{12}): ν(NC) 2152m, 2130sh, 2120s, ν(CO) 2051vw, 2032vs, 2019m, 2004m, 1997vs, 1989s, 1973w, 1869w, 1840m, 1789m, 1765s cm^{-1}. The fourth band was in trace amounts and could not be isolated.

3.7. Reaction of $Mo_2Ir_2(CO)_{10}(\eta\text{-}C_5H_5)_2$ with one equivalent of Bu^tNC

Following the procedure of Section 3.1, Bu^tNC (4 μl, 0.035 mmol) and **2** (34.7 mg, 0.035 mmol) in CH_2Cl_2 (15 ml) afforded a mixture which was applied to preparative TLC plates after 16 h reaction. Elution with CH_2Cl_2–petroleum (4/1) produced two bands. The first band (orange, $R_f = 0.74$) was in trace amounts and could not be isolated. The contents of the second band ($R_f = 0.55$) were crystallized from CH_2Cl_2–EtOH to afford deep purple crystals identified as $Mo_2Ir_2(\mu\text{-}CO)_2(CNBu^t)_2(CO)_6(\eta\text{-}C_5H_5)_2$ (**9**) (15.3 mg, 0.014 mmol, 80%). A crystal grown by this method was selected for a single-crystal X-ray structural study. IR (c-C_6H_{12}): ν(NC) 2157s, 2153sh, ν(CO) 2026m, 2016s, 1998vs, 1976m, 1962s, 1904m, 1887m, 1886m, 1837m, 1772m, 1751m cm^{-1}. ^{1}H-NMR ($CDCl_3$): δ 4.83 (s, 10H, C_5H_5), 1.46 (s, 18H, ^tBuNC) ppm. MS (FAB): 1097 ($[M]^+$, 16), 1069 ($[M-CO]^+$, 13), 1041 ($[M-2CO]^+$, 43), 1013 ($[M-3CO]^+$, 30), 985 ($[M-4CO]^+$, 77), 957 ($[M-5CO]^+$, 100), 929 ($[M-6CO]^+$, 24), 901 ($[M-7CO]^+$, 22), 873 ($[M-8CO]^+$, 15). Anal. Found: C, 30.68; H, 2.47; N, 2.87. $C_{28}H_{28}Ir_2Mo_2N_2O_8$ Calc: C, 30.66; H, 2.57; N, 2.55%.

3.8. Reaction of $Mo_2Ir_2(CO)_{10}(\eta\text{-}C_5H_5)_2$ with two equivalents of Bu^tNC

Following the procedure of Section 3.1, Bu^tNC (16 μl, 0.140 mmol) and **2** (69.4 mg, 0.070 mmol) in CH_2Cl_2 (20 ml) afforded a mixture which was applied to preparative TLC plates after 16 h reaction. Elution with CH_2Cl_2–petroleum (4/1) produced three bands. The orange contents of the first band ($R_f = 0.77$) were found to be unstable on the chromatography plates, giving an uncharacterizeable brown residue within minutes. The contents of the second band ($R_f = 0.60$) were identified as **9** (47.6 mg, 0.043 mmol, 62%) by solution IR. The dark brown contents of the third band ($R_f = 0.17$, 3.9 mg) were unstable in solution and formed a thick black residue within minutes.

3.9. Reaction of $Mo_2Ir_2(CO)_{10}(\eta\text{-}C_5H_5)_2$ with two equivalents of $CNC_6H_3Me_2$-2,6

Following the procedure of Section 3.1, $CNC_6H_3Me_2$-2,6 (13.2 mg, 0.101 mmol) and **2** (50.0 mg, 0.051 mmol) in CH_2Cl_2 (20 ml) afforded a mixture which was applied to preparative TLC plates after 16 h reaction. Elution with CH_2Cl_2–petroleum (4/1) produced three brown bands. The contents of the first band ($R_f = 0.85$) were identified as unreacted **2** (7.0 mg, 0.0071 mmol, 14%) by solution IR. The contents of the second band ($R_f = 0.69$) were crystallized from $CHCl_3$–MeOH to afford brown crystals identified as $Mo_2Ir_2(CNC_6H_3Me_2\text{-}2,6)(CO)_9(\eta\text{-}C_5H_5)_2$ (**10**) (15.6 mg, 0.014 mmol, 28%). IR (c-C_6H_{12}): ν(NC) 2148m, ν(CO) 2033vs, 2016s, 2001vs, 1980s, 1968m, 1921m, 1874m, 1851m, 1796w, 1763s cm^{-1}. ^{1}H-NMR ($CDCl_3$): δ 7.12 (m, 3H, C_6H_3), 4.90 (s, 10H, $2C_5H_5$), 2.42 (s, 6H, $C_6H_3Me_2$) ppm. MS (FAB): 1090 ($[M]^+$, 42), 1062 ($[M-CO]^+$, 34), 1034 ($[M-2CO]^+$, 100), 1006 ($[M-3CO]^+$, 36), 978 ($[M-4CO]^+$, 80), 950 ($[M-5CO]^+$, 89), 922 ($[M-6CO]^+$, 42), 894 ($[M-7CO]^+$, 37), 866 ($[M-8CO]^+$, 46), 851 ($[M-8CO-Me]^+$, 29), 838 ($[M-9CO]^+$, 38), 823 ($[M-9CO-Me]^+$, 18). Anal. Found: C, 30.82; H, 1.65; N, 1.20. $C_{28}H_{19}Ir_2Mo_2NO_9$ Calc: C, 30.86; H, 1.76; N, 1.29%. The third band ($R_f = 0.55$) was found to decompose slowly during development of the chromatography plates. The contents of the third band were purified from $CHCl_3$–MeOH to afford an amorphous brown solid tentatively identified as $Mo_2Ir_2(CNC_6H_3Me_2\text{-}2,6)_2(CO)_8(\eta\text{-}C_5H_5)_2$ (**11**) (10.3 mg, 0.0094 mmol, 17%). IR (c-C_6H_{12}): ν(NC) 2142s, 2116sh, ν(CO) 2025m, 2018vs, 1999s, 1987m, 1968s, 1959m, 1910m, 1893sh, 1862m, 1841m, 1782w, 1755s cm^{-1}. ^{1}H-NMR ($CDCl_3$): δ 7.10 (m, 6H, C_6H_3), 4.86 (s, 10H, C_5H_5), 2.40 (s, 12H, $C_6H_3Me_2$) ppm. TLC redevelopment of the contents of this band after 24 h gave three bands and a thick baseline. The first band was identified as **10** by solution IR. The second band ($R_f = 0.55$) behaved as **11**, decomposing on the chromatography plate. The third band ($R_f = 0.22$) was in trace amounts and could not be isolated.

3.10. X-ray crystallographic studies

The crystal and refinement data for compounds **3**, **6** and **9** are summarized in Table 2. Crystals suitable for X-ray structural analyses were grown by liquid diffusion techniques from CH_2Cl_2–MeOH (**3**) or CH_2Cl_2–EtOH (**6** and **9**) at 276 K. For each study, a single crystal was mounted on a fine glass capillary, and data collected on a Nonius Kappa CCD diffractometer using graphite monochromated Mo–K_α ($\lambda = 0.71069$ Å). The unit cell parameters were obtained by least-squares refinement [20] of N_{cell} reflections with $3^\circ \leq \theta \leq 30^\circ$ (**3** and **6**) or $3^\circ \leq \theta \leq 27^\circ$ (**9**). The reduced data [20] were corrected for absorption using numerical methods [21] implemented from within maXus [22]; equivalent reflections were merged. The structures were solved by heavy-atom Patterson methods [23] and expanded using Fourier techniques [24] within the software package teXsan [25].

The crystallographic asymmetric units for **3** and **6** consist of one molecule with all atoms in general position, whereas that for **9** contains one-half of a $[MoIr(\mu\text{-}CO)(CNBu^t)(CO)_3(\eta\text{-}C_5H_5)]_2$ dimer, with the other half being generated by a crystallographic twofold axis.

All non-hydrogen atoms in **6** and **9** were refined with anisotropic displacement parameters. For **3**, the methyl C atoms gave very elongated ellipsoids when refined as single sites with anisotropic displacement factors, and so they were each split over two sites of occupancy 0.5 with isotropic displacement parameters which were constrained to be equal. All other atoms were refined anisotropically. For **3**, restraints were placed on distances and angles about C(321) so that the C–C distances and N–C–C and C–C–C angles tended to their respective means. For all three structures, H atoms attached to C atoms were included in idealized positions and ride on the atoms to which they are bonded. The final cycles of matrix least-squares refinement were based on N_{obs} reflections and converged to R and R_w. The largest peaks in the final difference electron maps for all three structures are located near Ir atoms.

4. Supplementary material

Crystallographic data for the structural analyses have been deposited with the Cambridge Crystallographic Data Centre, CCDC Nos. 206437 (**6**), 206438 (**3**) and 206439 (**9**). Copies of this information may be obtained free of charge from the Director, CCDC, 12 Union Road, Cambridge CB2 1E2, UK (Fax: +44-1223-336033; e-mail: deposit@ccd.cam.ac.uk or www: http://www.ccdc.cam.ac.uk).

Acknowledgements

We thank the Australian Research Council (ARC) for financial support and Johnson-Matthey Technology Centre for the generous loan of iridium salts. M.G.H. holds an ARC Australian Senior Research Fellowship and A.J.U. held an ANU Honours Year Scholarship.

References

[1] E.G.A. Notaras, N.T. Lucas, M.G. Humphrey, A.C. Willis, A.D. Rae, Organometallics, in press.
[2] N.T. Lucas, J.P. Blitz, S. Petrie, R. Stranger, M.G. Humphrey, G.A. Heath, V. Otieno-Alego, J. Am. Chem. Soc. 124 (2002) 5139.
[3] J. Lee, M.G. Humphrey, D.C.R. Hockless, B.W. Skelton, A.H. White, Organometallics 12 (1993) 3468.
[4] S.M. Waterman, M.G. Humphrey, V.-A. Tolhurst, B.W. Skelton, A.H. White, D.C.R. Hockless, Organometallics 15 (1996) 934.
[5] N.T. Lucas, I.R. Whittall, M.G. Humphrey, D.C.R. Hockless, M.P.S. Perera, M.L. Williams, J. Organomet. Chem. 540 (1997) 147.
[6] N.T. Lucas, M.G. Humphrey, P.C. Healy, M.L. Williams, J. Organomet. Chem. 545–546 (1997) 519.
[7] S.M. Waterman, M.G. Humphrey, D.C.R. Hockless, J. Organomet. Chem. 555 (1998) 25.
[8] S.M. Waterman, M.G. Humphrey, D.C.R. Hockless, J. Organomet. Chem. 565 (1998) 81.
[9] S.M. Waterman, M.G. Humphrey, J. Lee, G.E. Ball, D.C.R. Hockless, Organometallics 18 (1999) 2440.
[10] S.M. Waterman, M.G. Humphrey, D.C.R. Hockless, J. Organomet. Chem. 582 (1999) 310.
[11] S.M. Waterman, M.G. Humphrey, J. Lee, J. Organomet. Chem. 589 (1999) 226.
[12] J.P. Blitz, N.T. Lucas, M.G. Humphrey, J. Organomet. Chem. 650 (2002) 133.
[13] S.M. Waterman, M.G. Humphrey, D.C.R. Hockless, J. Organomet. Chem. 579 (1999) 75.
[14] C.K. Johnson, ORTEP-II: a Fortran thermal ellipsoid plot program, Report ORNL-5138, Oak Ridge National Laboratory, Oak Ridge, TN, 1976.
[15] N.T. Lucas, M.G. Humphrey, D.C.R. Hockless, J. Organomet. Chem. 535 (1997) 175.
[16] R.J. Klingler, W.M. Butler, M.D. Curtis, J. Am. Chem. Soc. 100 (1978) 5034.
[17] M.D. Curtis, K.R. Han, W.M. Butler, Inorg. Chem. 19 (1980) 2096.
[18] D.F. Shriver, M.A. Drezdzon, The Manipulation of Air-sensitive Compounds, Wiley, New York, 1986.
[19] M.R. Churchill, Y.-J. Li, J.R. Shapley, D.S. Foose, W.S. Uchiyama, J. Organomet. Chem. 312 (1986) 121.
[20] Z. Otwinowski, W. Minor, in: C.W. Carter, Jr, R.M. Sweet (Eds.), Methods in Enzymology, Academic Press, New York, 1997, p. 307.
[21] P. Coppens, in: F.R. Ahmed, S.R. Hall, C.P. Huber (Eds.), Crystallographic Computing, Munksgaard, Copenhagen, 1970, p. 255.
[22] S. Mackay, C.J. Gilmore, C. Edwards, N. Stewart, K. Shankland, maXus: computer program for the solution and refinement of crystal structures, Nonius, The Netherlands, MacScience, Japan, and The University of Glasgow, UK, 1999.
[23] P.T. Beurskens, G. Admiraal, G. Beurskens, W.P. Bosman, S. Garcia-Granda, R.O. Gould, J.M.M. Smits, C. Smykalla, PATTY: the DIRDIF program system, Technical Report of the

Crystallography Laboratory, University of Nijmegen, Nijmegen, The Netherlands, 1992.
[24] P.T. Beurskens, G. Admiraal, G. Beurskens, W.P. Bosman, R. de Gelder, R. Israel, J.M.M. Smits, The DIRDIF-94 Program System, Technical Report of the Crystallography Laboratory, University of Nijmegen, Nijmegen, The Netherlands, 1994.
[25] M.S.C., teXsan: single-crystal structure analysis software, Version 1.8, The Woodlands, USA, 1997.